https://doi.org/10.5194/hess-2021-332
Preprint. Discussion started: 1 July 2021

Hydrology and Earth System Sciences
Open Access
Discussions

Easy-to-use spatial Random Forest-based downscaling-calibration method for producing high resolution and accurate precipitation data

Chuanfa Chen[1,2], Baojian Hu[1,2], Yanyan Li[1,2*]

[1] College of Geodesy and Geomatics, Shandong University of Science and Technology, Qingdao 266590, China

[2] Key Laboratory of Geomatics and Digital Technology of Shandong Province, Shandong University of Science and Technology, Qingdao 266590, China

* Correspondence: Yanyan Li (yylee@whu.edu.cn)

Abstract

High resolution and accurate precipitation data is significantly important for numerous hydrological applications. To enhance the spatial resolution and accuracy of satellite-based precipitation products, an easy-to-use downscaling-calibration method based on spatial Random Forest (SRF) is proposed in this paper, where the spatial autocorrelation between precipitation measurements is taken into account. The proposed method consists of two main stages. Firstly, the satellite-based precipitation was downscaled by SRF with the incorporation of some high-resolution covariates including latitude, longitude, DEM, NDVI, terrain slope, aspect, relief, and land surface temperatures. Then, the downscaled precipitation was calibrated by SRF with rain gauge observations and the aforementioned high-resolution variables. The monthly Integrated MultisatellitE Retrievals for Global Precipitation Measurement (IMERG) located in Sichuan province, China from 2015 to 2019 was processed using our method and its results were compared with those of some classical methods

https://doi.org/10.5194/hess-2021-332
Preprint. Discussion started: 1 July 2021

Hydrology and Earth System Sciences
Discussions

including geographically weighted regression (GWR), artificial neural network (ANN), random forest (RF), kriging interpolation only on gauge measurements, bilinear interpolation-based downscaling and then SRF-based calibration (Bi-SRF), and SRF-based downscaling and then geographical difference analysis (GDA)-based calibration (SRF-GDA). Results show that: (1) the proposed method outperforms the other methods as well as the original IMERG; (2) the monthly-based SRF estimation is slightly more accurate than the annual-based SRF fraction disaggregation method; (3) SRF-based downscaling and calibration preforms better than bilinear downscaling (Bi-SRF) and GDA-based calibration (SRF-GDA); (4) kriging seems more accurate than GWR and ANN in terms of quantitative accuracy measures, whereas its precipitation map cannot capture the detailed spatial precipitation patterns; and (5) among the predictors for calibration, the precipitation interpolated by kriging on the gauge measurements is the most important variable, indicating the significance for the inclusion of spatial autocorrelation information in gauge measurements.

Keywords: IMERG; Downscaling; Calibration; Machine learning; Interpolation

1. Introduction

Precipitation is an important variable for promoting our understanding of hydrological cycle and water resource management (Chen et al., 2010). Previous studies showed that about 70-80% of hydrological modeling errors were caused by precipitation data uncertainties (Gebregiorgis and Hossain, 2013). However, precipitation is also the most difficult meteorological factor to estimate due to its high

https://doi.org/10.5194/hess-2021-332
Preprint. Discussion started: 1 July 2021

spatial and temporal heterogeneity (Beck et al., 2019). Although rain gauge observations are reliable and accurate, it is difficult to reflect the spatial precipitation pattern with the sparse and uneven distribution and limited coverage, especially in remote and mountainous areas (Ullah et al., 2020).

During the past decades, plenty of satellite-based precipitation datasets have been produced at regional, quasi-global and fully global scales, such as the Climate Hazards Group Infrared Precipitation with Station data (CHIRPS, 0.05°) (Funk et al., 2015), the Precipitation Estimation from Remotely Sensed Information using Artificial Neural Networks-Climate Data Record (PERSIANN-CDR, 0.25°) (Ashouri et al., 2015), the Climate Prediction Center (CPC) morphing technique (CMORPH, 0.25°) (Haile et al., 2013), the Multi-Source Weighted-Ensemble Precipitation (MSWEP, 0.1°) (Beck et al., 2017), the Tropical Rainfall Measuring Mission (TRMM) Multi-satellite Precipitation Analysis (TMPA, 0.25°) (Huffman et al., 2007) and the Integrated MultisatellitE Retrievals for Global Precipitation Measurement (GPM) mission (IMERG, 0.1°) (Hou et al., 2014). Nevertheless, these products are characterized by considerable systematic biases due to the shortcomings of retrieval algorithms, sensor capability and spatiotemporal collection frequency (Chen et al., 2018; Wu et al., 2018; Yang et al., 2017). Moreover, their resolutions (from 0.05° to 2.5°) are too coarse to describe meso- and micro-scale precipitation patterns for hydrological studies at local and basin scales (Immerzeel et al., 2009). Hence, downscaling and calibration with the intention of improving the resolution and quality of satellite-based precipitation datasets has become an essential step prior to various

https://doi.org/10.5194/hess-2021-332
Preprint. Discussion started: 1 July 2021

hydrological applications at local scales (Bhuiyan et al., 2018).

Downscaling provides an effective way to derive high resolution precipitation products, which is generally achieved by constructing the relationship between precipitation and environmental variables at a coarse scale, and then putting the high-resolution variables into the constructed model to downscale the precipitation data from the coarse resolution to the fine (Chen et al., 2010; Immerzeel et al., 2009). At present, many downscaling models have been proposed. For example, Immerzeel et al. (2009) employed an exponential regression (ER) to describe the relationship between Tropical Rainfall Measuring Mission (TRMM) and Normalized Difference Vegetation Index (NDVI). Jia et al. (2011) used a multiple linear regression model (MLR) to establish the relationship between TRMM, digital elevation model (DEM) and NDVI. Duan and Bastiaanssen (2013) proposed a downscaling model based on the second-order polynomial relationship between TRMM and NDVI. Considering the heterogeneous relationship between precipitation and the land surface variables across the study areas, geographically weighted regression (GWR) was commonly adopted (Chen et al., 2015; Chen et al., 2014; Chen et al., 2020c; Li et al., 2019; Lu et al., 2020; Xu et al., 2015), and showed more accurate results than ER and MLR. In the recent decade, some data-driven machine learning (ML) methods such as random forests (RF) (Shi et al., 2015; Zhang et al., 2021), support vector machine (SVM) (Chen et al., 2010; Jing et al., 2016) and artificial neural network (ANN) (Elnashar et al., 2020) were employed to capture the complex nonlinear relationship between precipitation and the predictors. However, the downscaled precipitation products

https://doi.org/10.5194/hess-2021-332
Preprint. Discussion started: 1 July 2021

Hydrology and Earth System Sciences Discussions
Open Access
EGU

inevitably contain large systematic biases.

To alleviate the inherent biases, many calibration methods have been proposed for merging gauge observations and satellite-based precipitation to improve the accuracy and spatial coverage of precipitation, such as nonparametric kernel smoothing method (Li and Shao, 2010), geographical difference analysis (GDA) (Cheema and Bastiaanssen, 2012), geographical ratio analysis (GRA) (Duan and Bastiaanssen, 2013), conditional merging (CM) (Berndt et al., 2014), quantile mapping (Chen et al., 2013; Zhang and Tang, 2015), optimal interpolation (Lu et al., 2020; Wu et al., 2018; Xie and Xiong, 2011), GWR (Chao et al., 2018; Chen et al., 2018; Lu et al., 2019) and geostatistical interpolation (Park et al., 2017). However, these methods are based on some strict assumptions which might not be satisfied in practice (Wu et al., 2020; Zhang et al., 2021). Moreover, the precipitation-related environmental variables were not taken into account. To this end, ML-based calibration methods have become popular, such as Quantile Regression Forests (QRF) (Bhuiyan et al., 2018), ANN (Pham et al., 2020; Yang and Luo, 2014), deep neural network (Tao et al., 2016), RF (Baez-Villanueva et al., 2020), convolutional neural network (CNN) (Wu et al., 2020), SVM and extreme learning machine (Zhang et al., 2021). In contrast, RF with excellent results has been widely adopted in plenty of studies (Baez-Villanueva et al., 2020; Bhuiyan et al., 2020).

In the context of downscaling and calibration of precipitation data, the merits of the ML-based methods include (Hengl et al., 2018; Zhang et al., 2021): (i) they require no strict statistical assumptions; (ii) they can capture complex nonlinear relationship

https://doi.org/10.5194/hess-2021-332
Preprint. Discussion started: 1 July 2021

between precipitation and the environmental variables; (iii) they can include various types of predictors, without suffering from the collinearity problem and (iv) they are generally more accurate than the classical regression methods. However, there are at least two limitations: (i) the ML algorithms were simply taken as a statistical tool without considering the spatial autocorrelation between precipitation measurements; and (ii) the ML algorithms were adopted in either downscaling or calibration, without being used in both downscaling and calibration. More specifically, some (Jing et al., 2016; Karbalaye Ghorbanpour et al., 2021; Yan et al., 2021) attempted to use the ML methods for downscaling and then use the classical method (e.g. GDA and cokriging) for calibration, while some (Zhang et al., 2021) employed the classical interpolation methods (e.g. bilinear interpolation and kriging) for downscaling and then used the ML methods for calibration. However, we regard that the use of ML methods in both of downscaling and calibration could further improve the accuracy of precipitation, since the high resolution environmental variables with valuable information can be fully used in the two stages. To the best of our knowledge, no previous studies have used the ML technique in both downscaling and calibration with the consideration of high resolution environmental variables, simultaneously.

Based on aforementioned discussion, the objectives of this study are twofold: (i) to develop an easy-to-use spatial RF (SRF) by taking into account the spatial autocorrelation between adjacent gauge measurements, and (ii) to propose a downscaling-calibration method based on SRF for producing high resolution and accurate precipitation data. The use of RF as the basic model in our study is mainly due to its high interpolation accuracy and low computational cost (Belgiu et al., 2016; Mohsenzadeh Karimi et al., 2020).

Overall, the proposed method consists of two main steps. First, the precipitation data is downscaled by SRF with the incorporation of some environmental variables including DEM, NDVI, land surface temperatures (LSTs), terrain parameters, latitude and longitude as recommended in previous studies (Jing et al., 2016; Li et al., 2019). Second, SRF and the environmental variables were further used for merging the downscaled precipitation data and gauge observations to boost the accuracy of the precipitation data. The merit of the proposed method is that a new spatial RF is developed for both downscaling and calibration of precipitation products, with the incorporation of high-resolution environmental variables.

2 Study area and dataset

2.1. Study area

Sichuan province between 97°21'-108°31'E and 26°03'-34°19'N was selected as the study area (Fig. 1). It is situated between the Qinghai-Tibet Plateau and the Plain of the Middle-and-lower Reaches of Yangtze River, with an area of 486,000 km^2. Sichuan province has a complex and varied topography consisting of mountains, hills, plain basins and plateaus with the elevation ranging from approximately 180 m in the east to 7100 m in the west. Due to the different topographies in the west and east, the climate has a significant difference. The east basin has subtropical monsoon climate. The weather is generally warm, humid and foggy with much cloud, fog and rain but

https://doi.org/10.5194/hess-2021-332
Preprint. Discussion started: 1 July 2021

less sunshine. Most rain gathers from July to September, accounting for 80% of total annual precipitation. While in the west plateau, the weather is relatively cool or cold. The climate is featured by a long cold winter, a very short summer and rich sunshine but less rainfall. Thus, annual precipitation shows significant spatial heterogeneity, varying from about 400 mm in the west to 1800 mm in the east and with the average annual precipitation of about 1000 mm. Overall, the high spatial and temporal variability of precipitation with the complex topography makes the study site ideally suitable for the evaluation of satellite-based precipitation estimates.

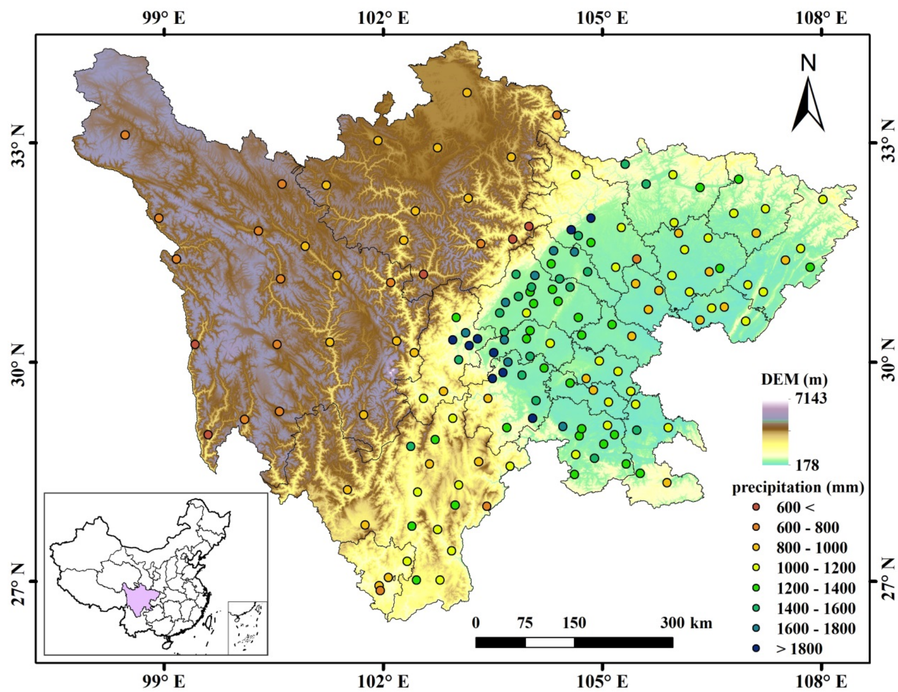

Fig. 1 Topography, distribution of rain gauges and geographic location of Sichuan province in China

2.2. Dataset

https://doi.org/10.5194/hess-2021-332
Preprint. Discussion started: 1 July 2021

2.2.1. Rain gauge observations

The study region has 156 rain gauge stations, which shows an unevenly distribution with high density in the east and low density in the west (Fig. 1). On average, the cover area of one rain gauge observation is about 3115 km^2. Daily precipitation data from all the stations for the period 2015–2019 were collected from the China Meteorological Data Service Center (CMDSC, http://data.cma.cn/). The data quality was guaranteed based on some strict quality controls, such as manual inspection, outlier check and spatiotemporal consistency verification (Zhao and Yatagai, 2014). After that, the monthly precipitation was produced by aggregating the daily precipitation of rain gauges for each month.

2.2.2. Integrated MultisatellitE Retrievals for Global Precipitation Measurement (IMERG)

As the successor of TRMM, the National Aeronautics and Space Administration (NASA) and the Japan Aerospace Exploration Agency (JAXA) initiated the next-generation global precipitation observation mission (Hou et al., 2014). The IMERG products were produced by assimilating all microwave and infrared (IR) estimates, together with gauge observations (Huffman et al., 2019). It has the spatial resolution of 0.1° × 0.1° with the coverage from 60°S-60°N. IMERG provides three different products including Early, Late, and Final Runs, which were computed about 4 hours, 14 hours, and 3.5 months after observation time, respectively. Due to the incorporation of the Global Precipitation Climatology Centre (GPCC) rain gauge data, IMERG Final Run is more accurate than the others (Lu et al., 2019). Thus, the

https://doi.org/10.5194/hess-2021-332
Preprint. Discussion started: 1 July 2021

Hydrology and Earth System Sciences
Open Access
Discussions

monthly IMERG V06B Final Run product was adopted in the study. It was downloaded from https://gpm.nasa.gov/data.

The mean monthly precipitations based on all rain gauges and IMERG during 2015-2019 are shown in Fig. 2. Obviously, IMERG has an overestimation in most months and the wettest month is July 2018.

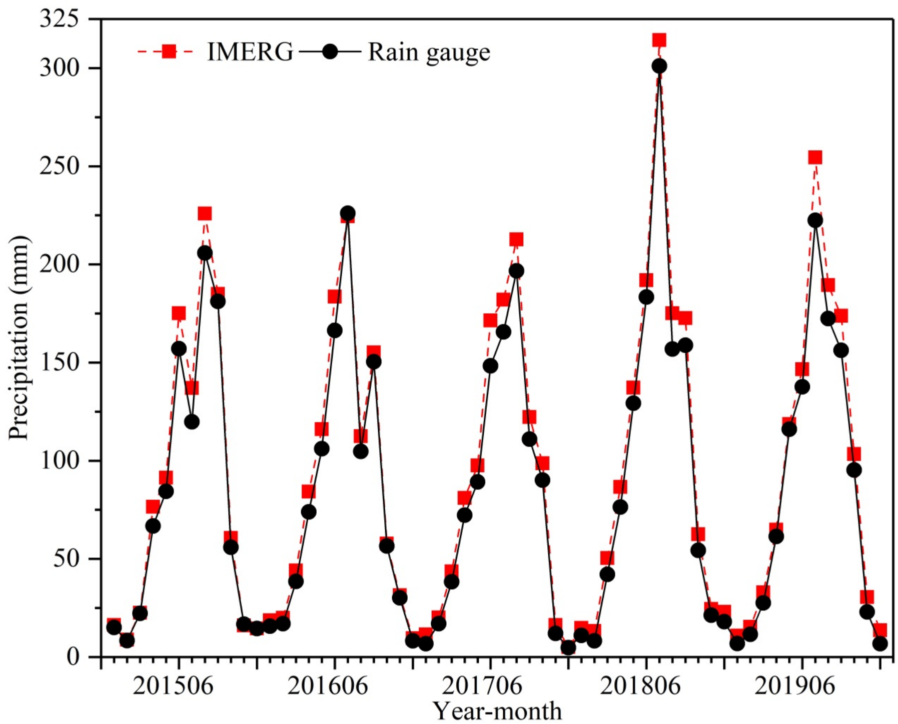

Fig. 2 Mean monthly precipitation based on rain gauges and IMERG from 2015-2019 over Sichuan province

2.2.3. Environmental variables

The Moderate Resolution Imaging Spectroradiometer (MODIS) onboard the NASA's Terra and Aqua platforms provides plenty of products in global dynamics, oceans and land processes. The MODIS monthly NDVI with the resolution of 1 km

https://doi.org/10.5194/hess-2021-332
Preprint. Discussion started: 1 July 2021

(MOD13A3) from 2015 to 2019 was used in the study and downloaded from International Scientific and Technical Data Mirror Site, Computer Network Information Center of the Chinese Academy of Sciences (http://www.gscloud.cn/). MODIS 8-day LST with the resolution of 1 km (MOD11A2) from 2015 to 2019 was obtained from https://ladsweb.modaps.eosdis.nasa.gov and then temporally averaged into the monthly LST products. In the study, the daytime LST (LST_D), nighttime LST (LST_N) and the difference between daytime and nighttime LSTs (LST_{D-N}) at the monthly scale were used.

The Shuttle Radar Topography Mission (SRTM) cooperated by the National Geospatial Intelligence Agency (NGA) and the National Aeronautics and Space Administration (NASA) provides high resolution DEMs. The SRTM DEM with the spatial resolution of 90 m was downloaded from http://srtm.csi.cgiar.org/ and then resampled to 1 km by the pixel averaging method. Moreover, topographical factors including slope, aspect and terrain relief (Chen et al., 2020a) were extracted from the SRTM DEM in ArcGIS 10.3.

The detailed information of the datasets used in the study is shown in Table 1.

Table 1 Datasets used in the study

Data Type	Product	Spatial resolution	Temporal resolution	Source
Meteorological data	GPM IMERG	10 km	Monthly	https://gpm.nasa.gov/data.
	Rain gauge observations	-	Daily	http://data.cma.cn/
Land surface	SRTM DEM	30 m	-	http://srtm.csi.cgiar.org/

https://doi.org/10.5194/hess-2021-332
Preprint. Discussion started: 1 July 2021

Hydrology and Earth System Sciences
Discussions

data	slope, aspect, terrain relief	30 m	-	Derived from SRTM DEM
	NDVI	1 km	Monthly	http://www.gscloud.cn/
	LST	1 km	8-days	https://ladsweb.modaps.eosdis.nasa.gov

3. Methodology

The flowchart of our method is demonstrated in Fig. 3, which includes three main stages: (i) data processing; (ii) IMERG downscaling and (iii) downscaled IMERG calibration. It is noted that downscaling before calibration is to avoid scale mismatch between satellite-based areal precipitation and gauge-based point measurements.

https://doi.org/10.5194/hess-2021-332
Preprint. Discussion started: 1 July 2021

Hydrology and Earth System Sciences
Open Access
Discussions

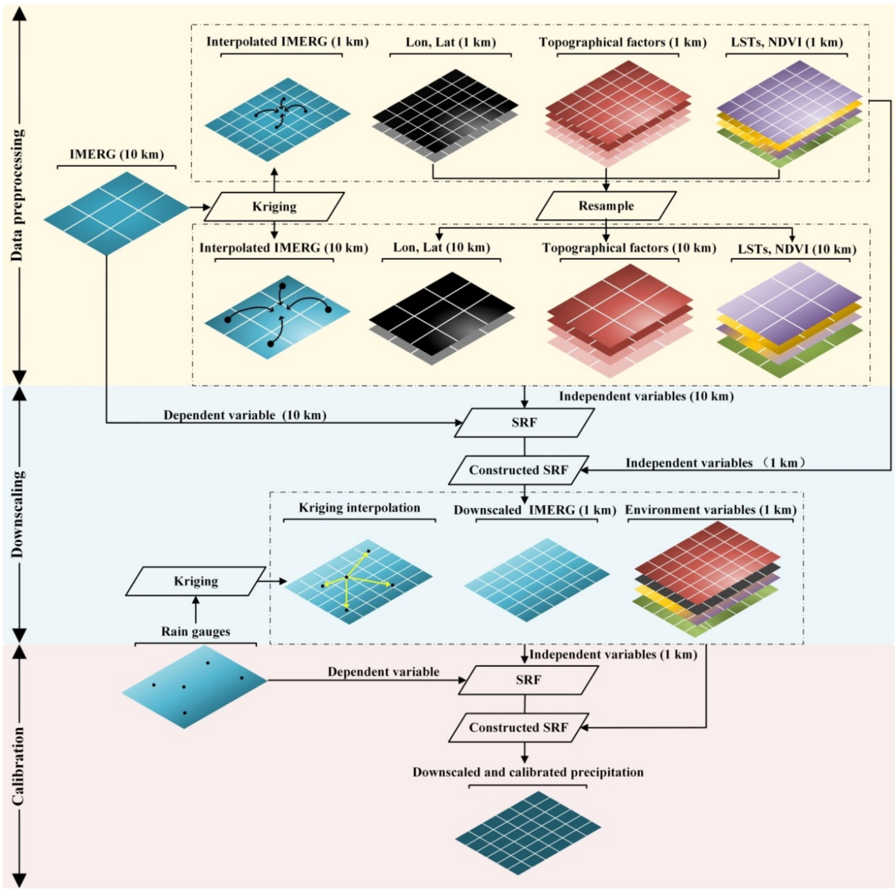

Fig. 3 Flowchart of the proposed method

3.1. Random Forest

RF is an ensemble of several tree predictors such that each tree relies on a random and independent selection of features but with the same distribution (Breiman, 2001). Specifically, each decision tree is constructed by randomly collecting some training data with replacement while the other is used to assess the tree (sample bagging). Moreover, while constructing each tree, only a random subset of features is selected at each decision node (feature bagging). In the end, the majority vote for classification

https://doi.org/10.5194/hess-2021-332
Preprint. Discussion started: 1 July 2021

Hydrology and Earth System Sciences
Discussions
Open Access
EGU

or the average prediction of all trees for regression is used to obtain the final output. Meanwhile, RF can evaluate the relative importance of the predictors by means of out-of-bag (OOB) observations. With the OOB error, the importance of each variable can be ranked. Many benchmarking researches have proven that RF is one promising ML technique currently available (Hengl et al., 2018). The general framework of RF is shown in Fig. 4.

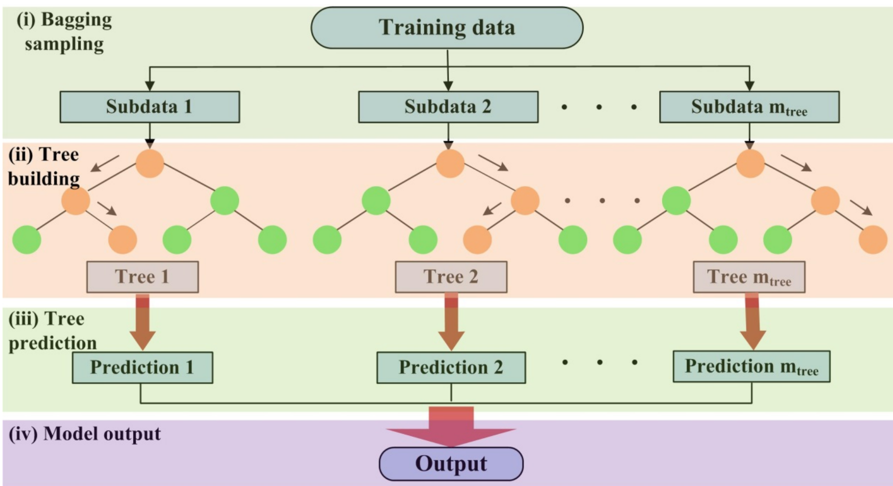

Fig. 4 General framework of RF

3.2. Spatial Random Forest (SRF)

In essence, the classical RF is a non-spatial statistical technique for spatial prediction since it neglects sampling locations and general sampling pattern (Hengl et al., 2018). This can potentially cause sub-optimal estimations, especially when the spatial autocorrelation between dependent variables is high. To this end, a spatial RF is proposed in this paper. The general formulation of SRF is as follows:

https://doi.org/10.5194/hess-2021-332
Preprint. Discussion started: 1 July 2021

$$\hat{p}(\boldsymbol{s}_0) = f(\boldsymbol{X}_s, \boldsymbol{X}_{ns}) + e$$

where $\hat{p}$ is the estimated precipitation at the location $\boldsymbol{s}_0$, e is the fitting residual, and $\boldsymbol{X}_s$ and $\boldsymbol{X}_{ns}$ are the spatial and non-spatial covariates, respectively.

In addition to spatial coordinates, one spatial covariate (X_s) is estimated to account for the spatial autocorrelation between neighboring precipitation measurements, i.e.

$$X_s(\boldsymbol{s}_0) = \sum_{i=1}^{n} w_i z(\boldsymbol{s}_i)$$

where $z(\boldsymbol{s}_i)$ is the ith neighboring precipitation data of the unknown point $\boldsymbol{s}_0$, w_i is its weight and n is the number of known data used for the estimation.

In previous studies (Li et al., 2017; Zhang et al., 2021), the inverse distance weights (IDW) were commonly used. However, the IDW method only resorts to the spatial distance between the estimated point and the adjacent known points, and does not consider the spatial autocorrelation between the known points. To overcome this limitation, the ordinary kriging-based variogram is adopted to estimate the interpolation weights, which are obtained by solving the following linear system:

$$\begin{pmatrix} \gamma(\boldsymbol{x}_1 - \boldsymbol{x}_1) & \cdots & \gamma(\boldsymbol{x}_1 - \boldsymbol{x}_n) & 1 \\ \vdots & \ddots & \vdots & \vdots \\ \gamma(\boldsymbol{x}_n - \boldsymbol{x}_1) & \cdots & \gamma(\boldsymbol{x}_n - \boldsymbol{x}_n) & 1 \\ 1 & \cdots & 1 & 0 \end{pmatrix} \begin{pmatrix} w_1 \\ \vdots \\ w_n \\ \mu \end{pmatrix} = \begin{pmatrix} \gamma(\boldsymbol{x}_1 - \boldsymbol{x}_0) \\ \vdots \\ \gamma(\boldsymbol{x}_n - \boldsymbol{x}_0) \\ 1 \end{pmatrix}$$

where μ is Lagrange parameter and $\gamma(\cdot)$ is the semivariogram.

It can be concluded that the variogram-based weights consider the spatial autocorrelation not only between the adjacent known points but also between the known points and the interpolated point (Berndt and Haberlandt, 2018). Thus, it seems more accurate than IDW. In practice, the experimental semivariogram is

https://doi.org/10.5194/hess-2021-332
Preprint. Discussion started: 1 July 2021

estimated from sample data with the following equation (Goovaerts, 2000):

$$\hat{\gamma}(h)=\frac{1}{2n}\sum_{i=1}^{n}\left(z\left(\boldsymbol{x}_i\right)-z\left(\boldsymbol{x}_i+h\right)\right)^2$$

where n is the number of data pairs with the attribute z separated by distance h.

Generally, a theoretical semivariogram model was fitted to the experimental values to obtain the semivariogram at any h. There are four commonly used theoretical semivariogram models: the spherical, Gaussian, exponential, and power models. In our study, the spherical model was used since it shows better results than the others in the experiments.

3.3. Working procedure of the proposed method

The detailed steps of the proposed method are as follows (Fig. 3):

(1) Each pixel value of the 10 km IMERG was re-estimated by ordinary kriging interpolation with its k nearest neighbors (e.g. k=8) to obtain the interpolated IMERG (termed as $I_s^{10\mathrm{km}}$), the 10 km IMERG was interpolated by kriging to obtain the interpolated 1 km IMERG ($I_s^{1\mathrm{km}}$), and the gauge observations are interpolated by kriging to produce the 1 km precipitation map ($P_s^{1\mathrm{km}}$). It is noted that the semivariogram model cannot be accurately estimated from the sparse gauge measurements. Hence, it is difficult to accurately show the spatial autocorrelation between the precipitation estimates. Motivated by the idea of Chen et al. (2020c) that the satellite-based precipitation can show the spatial distribution of precipitation, we used the satellite-based precipitation to estimate the experimental semivariogram for interpolating gauge measurements.

https://doi.org/10.5194/hess-2021-332
Preprint. Discussion started: 1 July 2021

(2) The negative NDVI values were excluded from the original data, which mainly belong to snow and water bodies in the study site. The removed ones were estimated by kriging with their neighbors, which can avoid much information loss.

(3) The 1 km environmental variables $\boldsymbol{X}_{ns}^{1\mathrm{km}}$ (i.e. NDVI, LST_D, LST_N, $LST_{D\text{-}N}$, DEM, slope, aspect, terrain relief, latitude and longitude) were resampled to the 10 km resolution $\boldsymbol{X}_{ns}^{10\mathrm{km}}$ by the pixel averaging method.

(4) The relationship between $\boldsymbol{X}_{ns}^{10\mathrm{km}}$, $I_s^{10\mathrm{km}}$ and the 10 km IMERG ($IMERG^{10\mathrm{km}}$) was constructed by SRF:

$$IMERG^{10\mathrm{km}}(\boldsymbol{s}_0) = f_{\mathrm{downscale}}\left(I_s^{10\mathrm{km}}(\boldsymbol{s}_0), \boldsymbol{X}_{ns}^{10\mathrm{km}}(\boldsymbol{s}_0)\right) + e^{10\mathrm{km}}(\boldsymbol{s}_0)$$

where e is the fitting residual.

(5) The IMERG was downscaled to 1 km ($\hat{D}^{1\mathrm{km}}$) by the constructed relationship in step (4) with $\boldsymbol{X}_{ns}^{1\mathrm{km}}$ and $I_s^{1\mathrm{km}}$:

$$\hat{D}^{1\mathrm{km}} = f_{\mathrm{downscale}}\left(I_s^{1\mathrm{km}}, \boldsymbol{X}_{ns}^{1\mathrm{km}}\right)$$

(6) The relationship between the 1 km predictors and the gauge observations (G) are constructed by SRF:

$$G(\boldsymbol{s}_0) = f_{\mathrm{calibrate}}\left(P_s^{1\mathrm{km}}(\boldsymbol{s}_0), \hat{D}^{1\mathrm{km}}(\boldsymbol{s}_0), \boldsymbol{X}_{ns}^{1\mathrm{km}}(\boldsymbol{s}_0)\right) + e^{1\mathrm{km}}(\boldsymbol{s}_0)$$

(7) The 1 km high quality precipitation data ($C^{1\mathrm{km}}$) are produced based on the constructed relationship in step (6):

$$C^{1\mathrm{km}} = f_{\mathrm{calibrate}}\left(P_s^{1\mathrm{km}}, \hat{D}^{1\mathrm{km}}, \boldsymbol{X}_{ns}^{1\mathrm{km}}\right)$$

In our study, residual correction was ignored during downscaling and calibration, since many previous studies (Karbalaye Ghorbanpour et al., 2021; Lu et al., 2019) demonstrated that residual correction on the ML-based technique decreased the

https://doi.org/10.5194/hess-2021-332
Preprint. Discussion started: 1 July 2021

prediction accuracy.

3.4. Comparative methods

In the study, the performance of our method was comparatively assessed using three manners. Firstly, we compared the results of the proposed method with those of the classical methods including GWR, RF and BPNN. Secondly, our methodology was compared with two classical frameworks: (i) the IMERG was downscaled by the bilinear interpolation and then calibrated by SRF (termed as Bi-SRF), and (ii) the IMERG was downscaled by SRF and then calibrated by GDA (termed as SRF-GDA). Thirdly, our monthly-based estimation method was compared with the annual-based SRF fraction disaggregation method (termed as SRFdis). Finally, the results of our method were compared with that from ordinary kriging interpolation only on gauge measurements (termed as kriging). Overall, the proposed method was compared with seven classical methods in our study, including GWR, RF, BPNN, Bi-SRF, SRF-GDA, SRFdis and kriging.

Note that the parameters of all the methods were tuned based on the trial-and-error scheme under the *l*-fold cross validation technique (An et al., 2007). Specifically, all gauge measurements were first divided into *l* folds. The prediction function was trained using *l*-1 folds, and the remainder was used for validation. The process is repeated *l* times until all folds were used for validation. Here, we set *l*=10. For each group of specified parameters, the 10-fold cross validation was repeated for one time, and the optimized parameters correspond to the minimized fitting error. Thus, the

https://doi.org/10.5194/hess-2021-332
Preprint. Discussion started: 1 July 2021

overfitting problem could be avoided.

3.5. Accuracy measures

Three accuracy measures were adopted in the quantitative accuracy evaluation, including root mean square error (RMSE), mean absolute error (MAE) and correlation coefficient (CC) (Jing et al., 2016; Sharifi et al., 2019). They are respectively expressed as

$$RMSE = \sqrt{\frac{1}{n}\sum_{i=1}^{n}\left(E_i - O_i\right)^2}$$

$$MAE = \frac{\sum_{i=1}^{n}\left|E_i - O_i\right|}{n}$$

$$CC = \frac{\sum_{i=1}^{n}\left(E_i - \bar{E}\right)\left(O_i - \bar{O}\right)}{\sqrt{\sum_{i=1}^{n}\left(E_i - \bar{E}\right)^2} \times \sqrt{\sum_{i=1}^{n}\left(O_i - \bar{O}\right)^2}}$$

where n is the number of testing stations, E_i and O_i are the estimated and observed precipitations at station i, respectively.

Generally, CC is used to measure the consistency between the estimated and observed precipitations, while RMSE and MAE can assess the absolute deviation between the estimated and observed values.

4. Results and analysis

We analyzed the results of the proposed method and the other methods on different temporal scales including monthly, seasonal and annual ones, where the latter two

https://doi.org/10.5194/hess-2021-332
Preprint. Discussion started: 1 July 2021

Hydrology and Earth System Sciences Discussions
Open Access

scales were averagely computed from the monthly one.

4.1. Monthly scale

Fig. 5 illustrates the scatterplots between the predicted and observed precipitations on a monthly scale from 2015 to 2019. Results demonstrate that regardless of accuracy measures, BPNN and GWR produce worse results than the original IMERG. This is mainly owed to the complex relationship between the precipitation and the predictors, which was not accurately captured by the two methods. RF performs better than IMERG, yet worse than kriging. By contrast, the four SRF-based methods including the proposed method, Bi-SRF, SRF-GDA and SRFdis outperform the other methods. This reflects the significant effect of spatial autocorrelation between the gauge measurements on capturing the complex predictors-precipitation relationship. Moreover, the proposed method with the RMSE, MAE and CC of 33.22 mm, 19.22 mm and 0.933 produces the best result. Thus, it can be concluded that (i) SRF-based downscaling and calibration is more effective than bilinear downscaling (Bi-SRF) and GDA-based calibration (SRF-GDA) and (ii) there is no obvious time latency for vegetation response to precipitation in the study site, since the proposed method is slightly more accurate than SRFdis.

https://doi.org/10.5194/hess-2021-332
Preprint. Discussion started: 1 July 2021

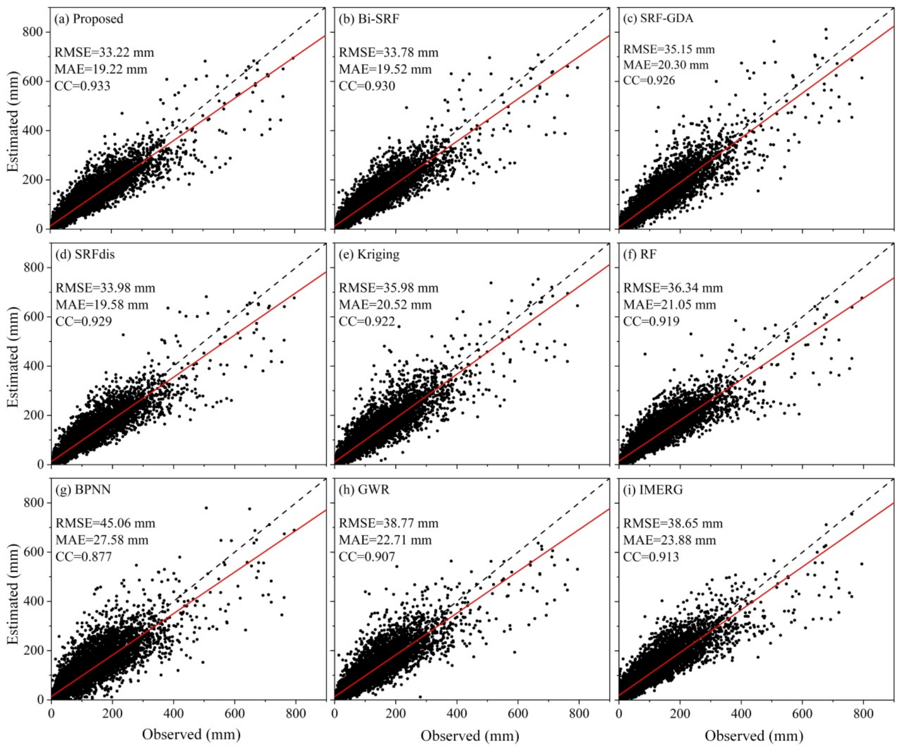

Fig. 5 Scatterplots between the estimated and the observed precipitation on a monthly scale from 2015 to 2019

Fig. 6 shows the boxplots of the four accuracy measures. Obviously, BPNN obtains the poorest results, with the median RMSE, MAC and CC of 30.48 mm, 22.66 mm and 0.64, respectively. It is followed by GWR, RF and kriging. The accuracy rank is consistent with that shown in Fig. 5. The four methods based on SRF seem more accurate than the classical methods. SRFdis, Bi-SRF and SRF-GDA have the median RMSEs of 21.41, 21.44 and 22.27 mm, respectively, while the proposed method has the value of 21.03 mm. In other words, the proposed method outperforms the other methods, which further highlights the benefit of including spatial autocorrelation information for downscaling and calibration of satellite-based precipitation.

https://doi.org/10.5194/hess-2021-332
Preprint. Discussion started: 1 July 2021

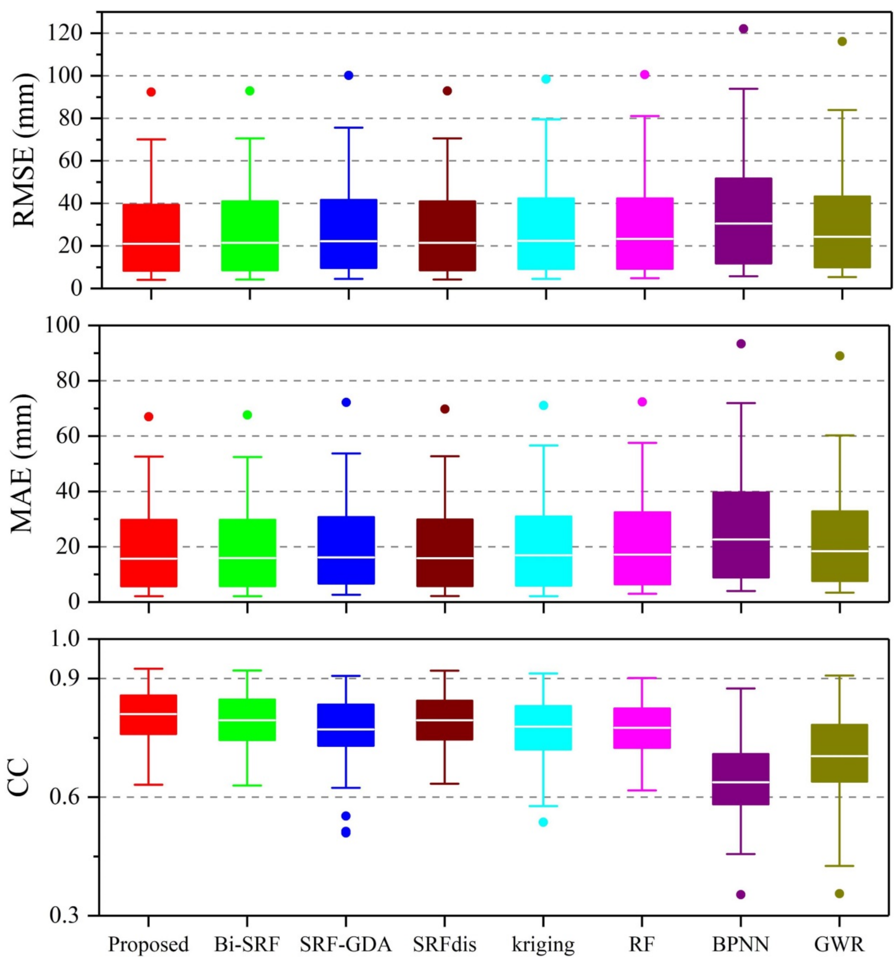

Fig. 6 Boxplots of RMSE, MAE and CC for the precipitation estimation methods on a monthly scale during 2015-2019

Fig. 7 shows the RMSE spatial distribution of all gauge stations for the proposed method, SRFdis, RF, BPNN, kriging and GWR. Overall, the RMSEs tend to be larger in the middle part, since the precipitation is higher in the middle part than in the other parts (Fig. 1). BPNN (Fig. 7d) yields the poorest results, where many stations have the RMSEs greater than 60 mm. It is followed by GWR (Fig. 7f). RF (Fig. 7c) and kriging (Fig. 7e) seem better than GWR and BPNN at most stations. The proposed method (Fig. 7a) and SRFdis (Fig. 7b) are more accurate than the classical methods, especially at the stations in the middle area. Moreover, the proposed method performs better than SRFdis at some stations, such as those in the right-top.

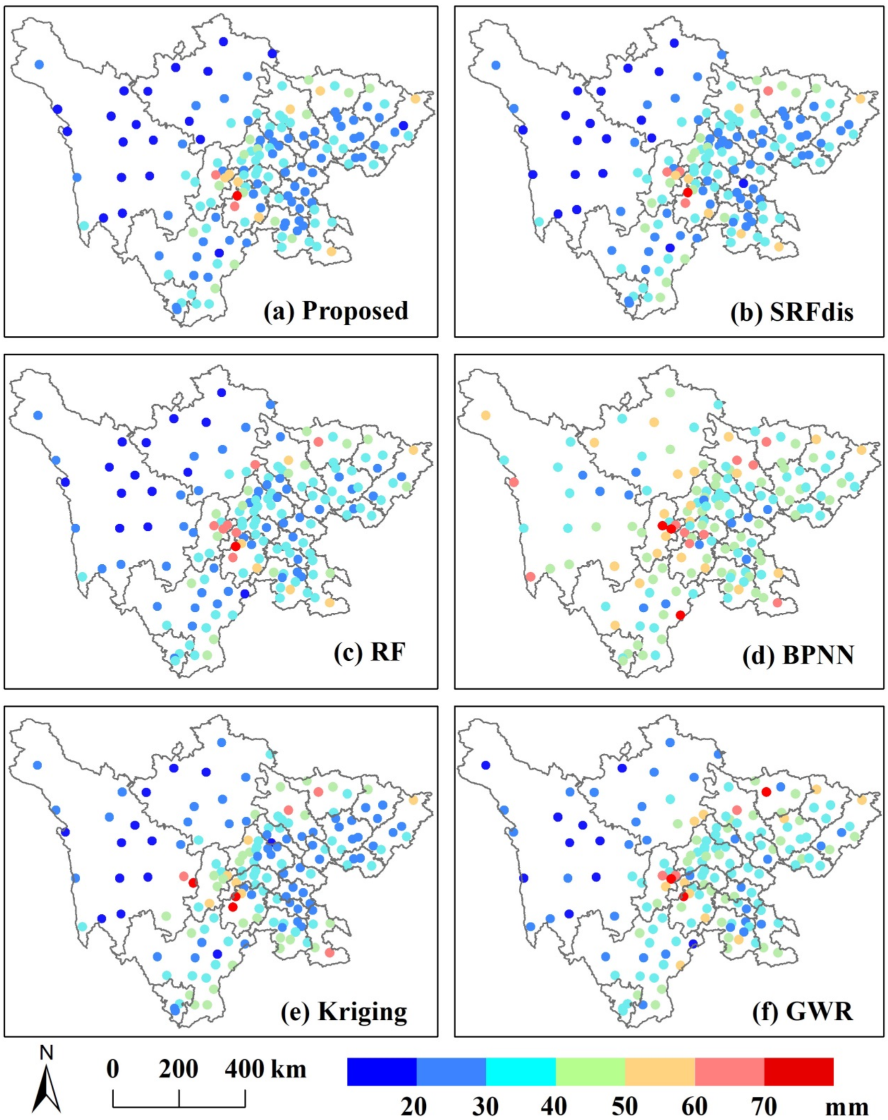

Fig. 7 RMSE distribution of all gauge stations for the proposed method and some representative methods on a monthly scale during 2015-2019

https://doi.org/10.5194/hess-2021-332
Preprint. Discussion started: 1 July 2021

4.2. Seasonal scale

The estimation errors of all the methods on a seasonal scale (i.e. spring, summer, autumn and winter) are provided in Table 2. Results indicate that regardless of accuracy measures, all methods obtain the best and the worst results in winter and in summer, respectively. This conclusion is consistent with the results yielded by (Baez-Villanueva et al., 2020; Chen et al., 2020c; Zambrano-Bigiarini et al., 2017). This could be due to the facts that (i) winter has the lowest precipitation and summer has the highest one (Fig. 2), and (ii) the large precipitation in summer was caused by complex conditions, like climatic anomaly and encounter of the cold and warm air masses, which cannot be accurately explained by the predictors (Chen et al., 2015). The accuracy rank for all the methods in the four seasons is similar. More specifically, BPNN yields worse results than IMERG in spring, summer and autumn, and a better result in winter. GWR is slightly more accurate than BPNN in the four seasons. Kriging with a similar accuracy to RF obviously outperforms BPNN and GWR. The four SRF-based methods seem more accurate than the classical methods in almost all seasons, expect for SRF-GDA in winter. Moreover, the proposed method consistently performs the best in the four seasons. Taking winter as an example, our method is about 11.44%, 8.59%, 4.77% and 2.89% more accurate than kriging, RF, BPNN and GWR, respectively.

Table 2 RMSEs, MAEs and CCs of all the estimation methods on a seasonal scale during 2015-2019 (RMSE: mm; MAE: mm)

https://doi.org/10.5194/hess-2021-332
Preprint. Discussion started: 1 July 2021

Hydrology and Earth System Sciences
Open Access
EGU
Discussions

Season	Index	Proposed	Bi-SRF	SRF-GDA	SRFdis	Kriging	RF	BPNN	GWR	IMERG
Spring	RMSE	21.99	22.19	23.03	22.04	23.38	23.67	30.71	25.97	25.97
	MAE	15.36	15.52	15.93	15.48	16.14	16.64	22.48	18.24	19.30
	CC	0.889	0.887	0.882	0.888	0.876	0.870	0.793	0.841	0.855
Summer	RMSE	56.13	57.06	59.27	57.51	61.07	61.83	74.46	65.49	64.46
	MAE	39.92	40.44	41.77	40.63	43.16	43.66	54.55	46.32	47.30
	CC	0.857	0.851	0.845	0.849	0.832	0.824	0.745	0.795	0.818
Autumn	RMSE	27.50	28.06	29.23	28.24	29.49	29.48	39.70	31.63	32.19
	MAE	17.51	17.89	18.53	17.96	18.42	19.25	26.67	20.79	21.98
	CC	0.928	0.925	0.920	0.924	0.918	0.917	0.864	0.902	0.905
Winter	RMSE	6.29	6.54	7.70	6.51	7.01	6.83	9.29	8.11	11.28
	MAE	4.11	4.25	4.97	4.26	4.36	4.65	6.64	5.66	6.93
	CC	0.853	0.839	0.790	0.841	0.823	0.826	0.688	0.735	0.595

To further illustrate the distributions of each accuracy measure, the boxplots of RMSEs, MAEs and CCs in each season are provided in Figs. 8, 9 and 10, respectively. Obviously, BPNN has the largest accuracy range in the four seasons, indicating its instability for precipitation estimation. Moreover, it produces the largest median RMSEs and MAEs with the values of 9.23-71.25 mm and 6.90-55.42 mm, respectively, and the smallest median CCs with the values of 0.61-0.66. Compared to BPNN, the RMSEs of RF and GWR are decreased to 6.90-54.92 mm and 7.04-58.17 mm, respectively, MAEs to 4.67-40.10 mm and 5.02-41.48 mm, respectively, while CCs are increased to 0.76-0.80 and 0.39-0.73, respectively. Kriging performs better

https://doi.org/10.5194/hess-2021-332
Preprint. Discussion started: 1 July 2021

than RF and GWR in almost all seasons, except for summer. Except for SRF-GDA, the other SRF-based methods are more accurate than the classical methods. On the whole, the proposed method produces the best results, with the median RMSEs, MAEs and CCs of 6.35-52.08 mm, 4.18-38.94 mm and 0.78-0.84 in the four seasons.

https://doi.org/10.5194/hess-2021-332
Preprint. Discussion started: 1 July 2021

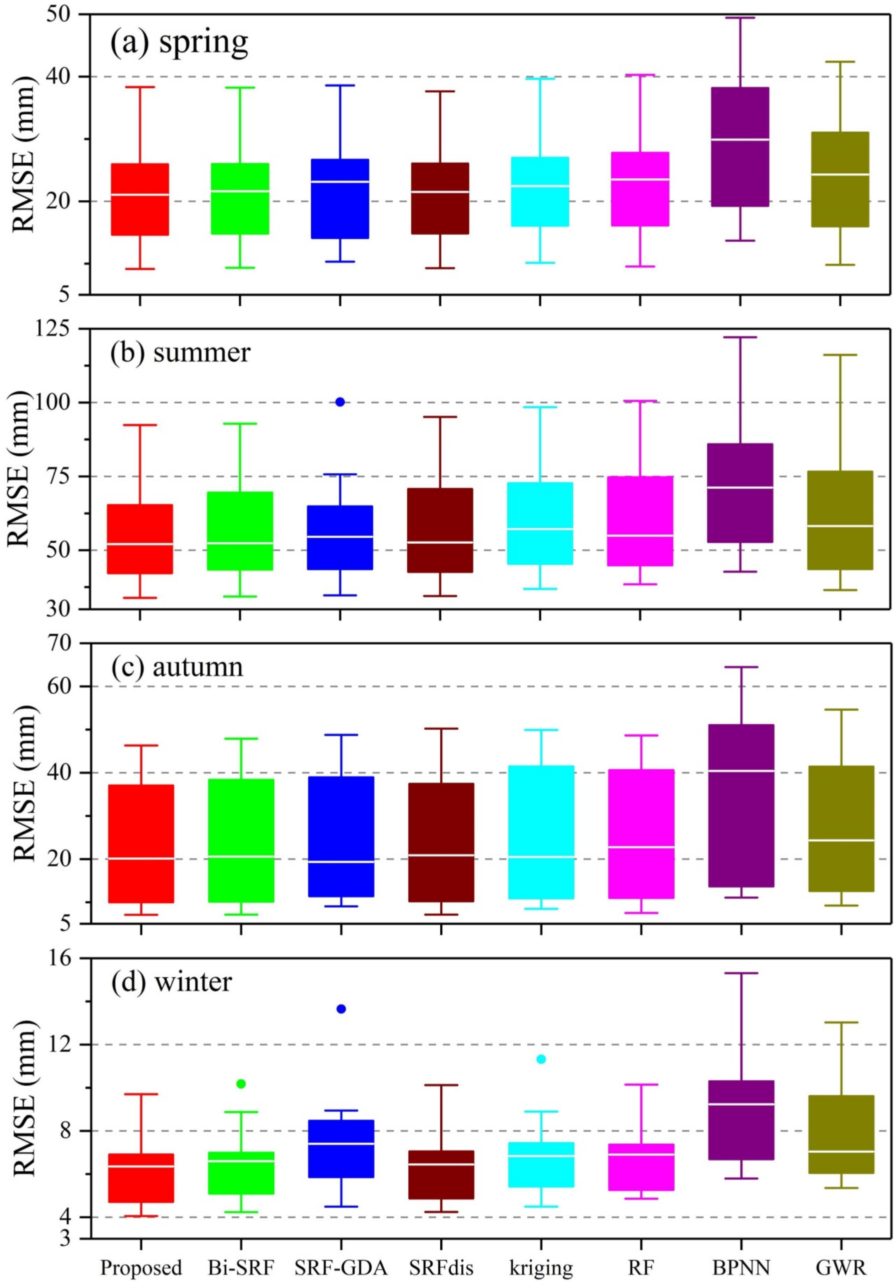

Fig. 8 Boxplots of RMSEs of all the methods on the seasonal scale during 2015-2019

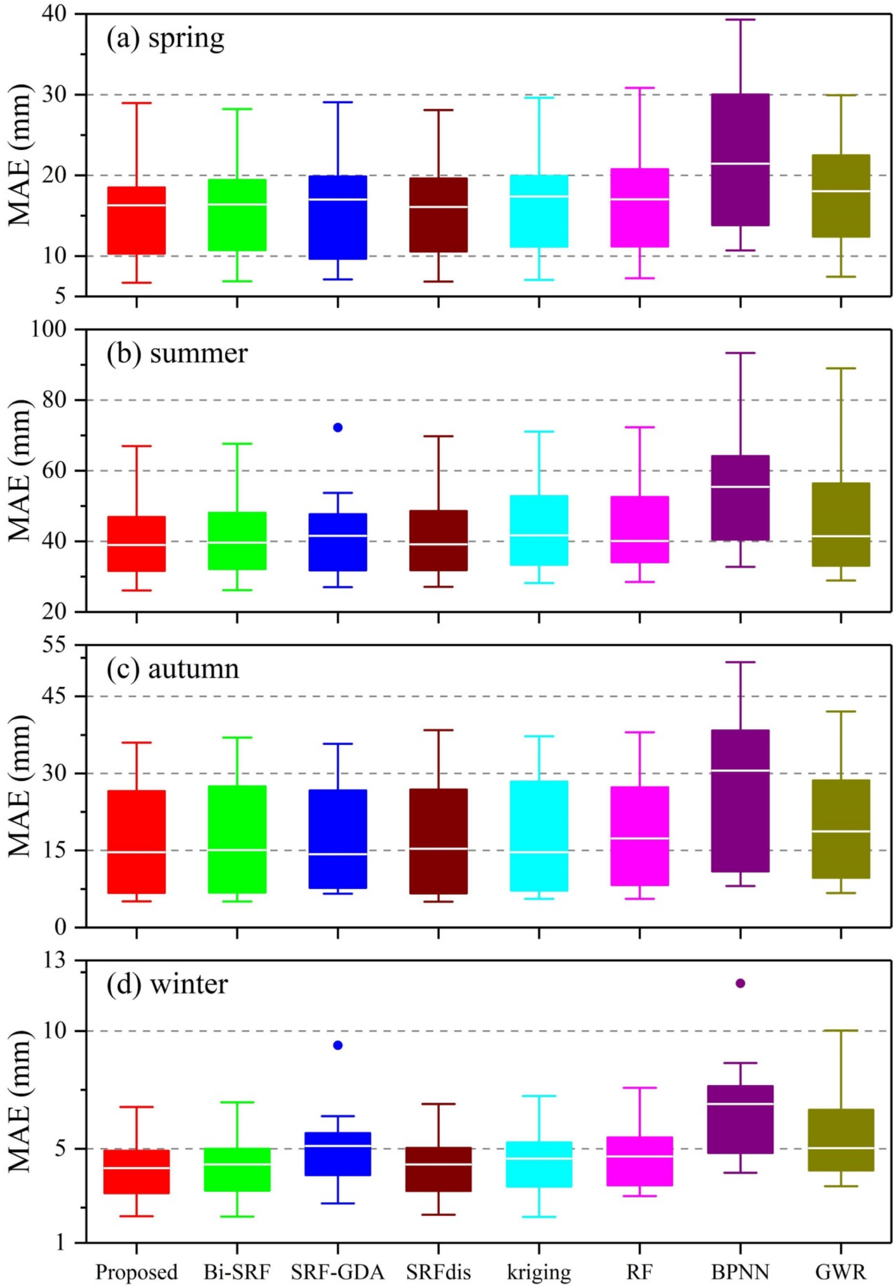

426 Fig. 9 Boxplots of MAEs of all the methods on the seasonal scale during 2015-2019

https://doi.org/10.5194/hess-2021-332
Preprint. Discussion started: 1 July 2021

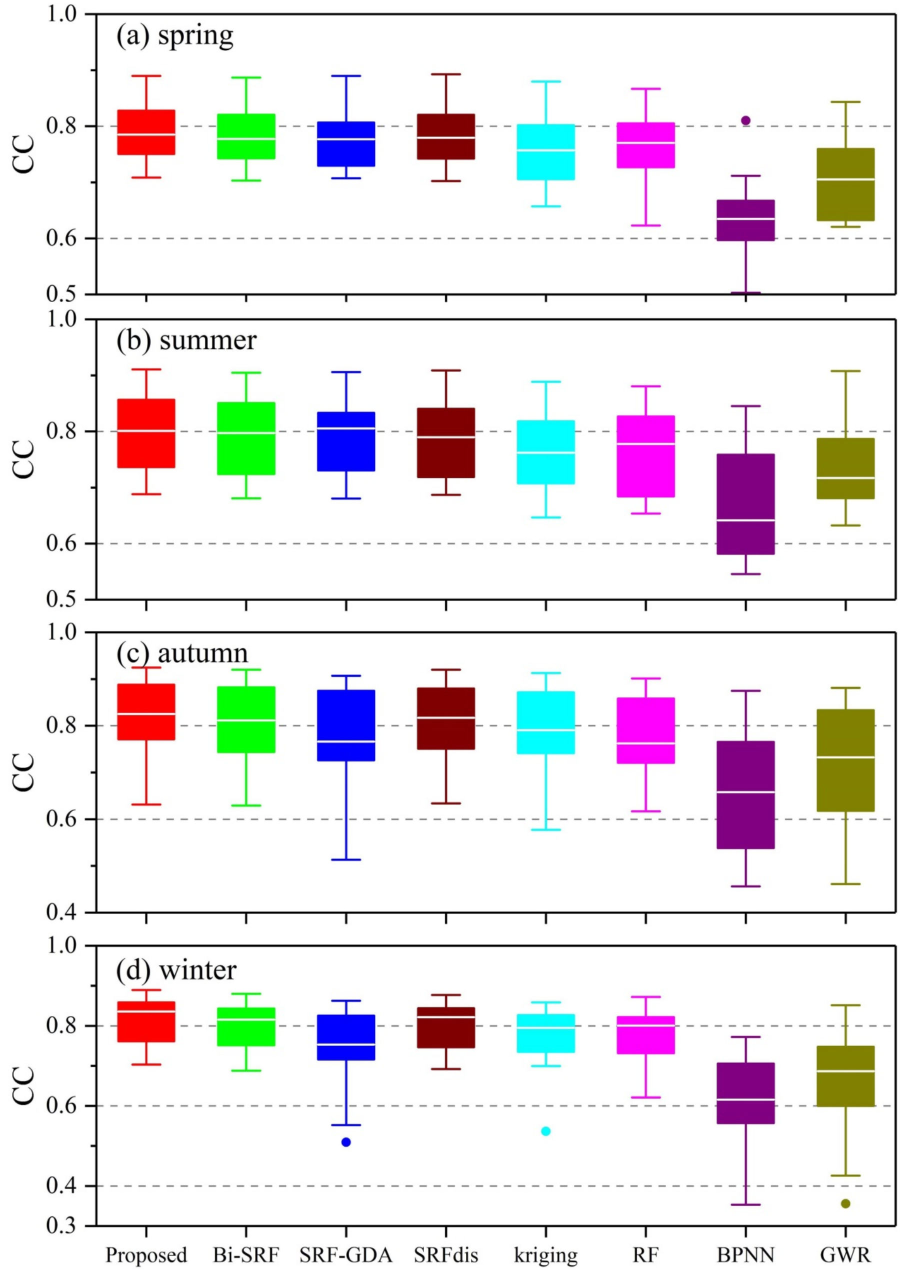

Fig. 10 Boxplots of CCs of all the methods on the seasonal scale during 2015-2019

4.3. Annual scale

Fig. 11 illustrates the accuracy measures of all the methods on an annual scale from 2015 to 2019. Results demonstrate that all methods produce the worst results in 2018. This is because this year has the largest precipitation (Fig. 2). In comparison, BPNN produces the poorest results in all years, which is followed by IMERG and GWR. RF and kriging are consistently more accurate than BPNN, IMERG and GWR, especially in 2017-2019. The proposed method always performs better than the other methods in the five years, which is closely followed by Bi-SRF and SRFdis. SRF-GDA produces worse results than the other SRF-based methods.

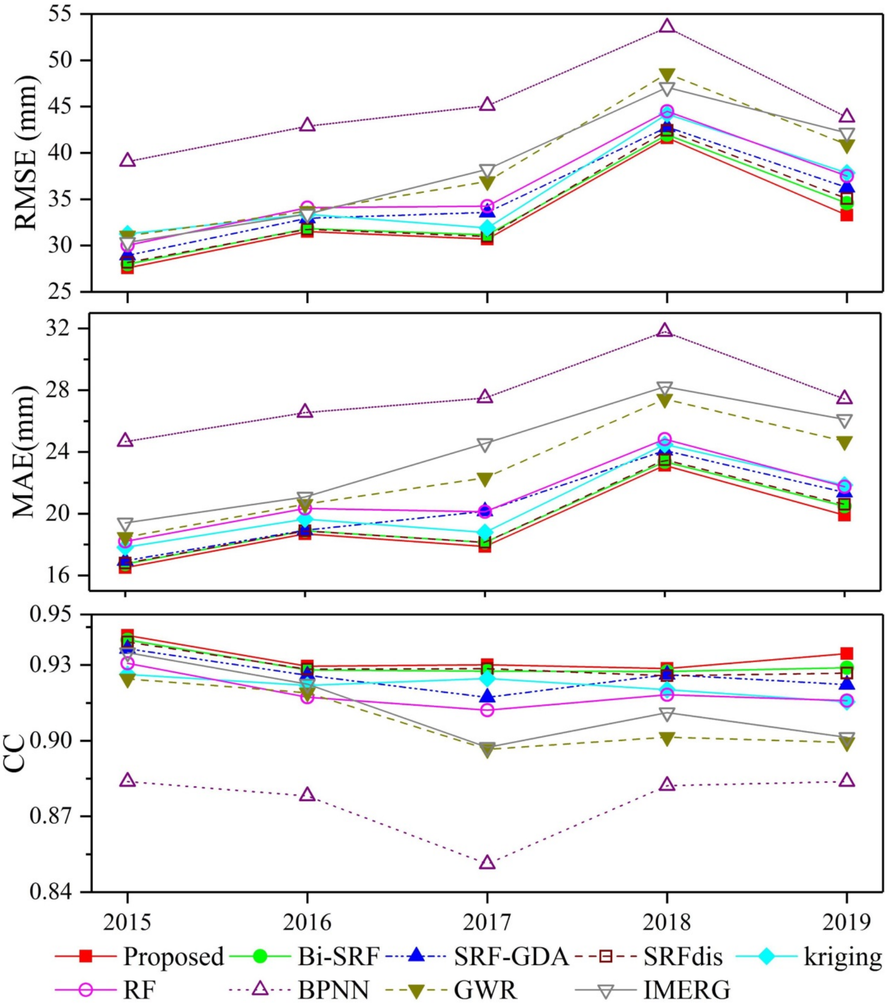

Fig. 11 Accuracy measures of all the methods on an annual scale from 2015 to 2019

Since the wettest month was July 2018 (Fig. 2), it was taken as an example to show the precipitation estimates of the proposed method and some classical methods. Results (Fig. 12) indicate that all the estimated precipitation maps have a similar spatial distribution and pattern to IMERG, yet the former have more detailed information than the latter due to the inclusion of the high-resolution predictors. However, there exist some differences between the methods. Specifically, the kriging

https://doi.org/10.5194/hess-2021-332
Preprint. Discussion started: 1 July 2021

map (Fig. 12b) loses many details of spatial precipitation patterns. This is expected as it only uses ground measurements for the interpolation. RF (Fig. 12c) shows obvious unnatural discontinuity. GWR (Fig. 12d) suffers from more variations and fractions compared with neighbors. In comparison, the proposed method (Fig. 12a) produces a good precipitation map.

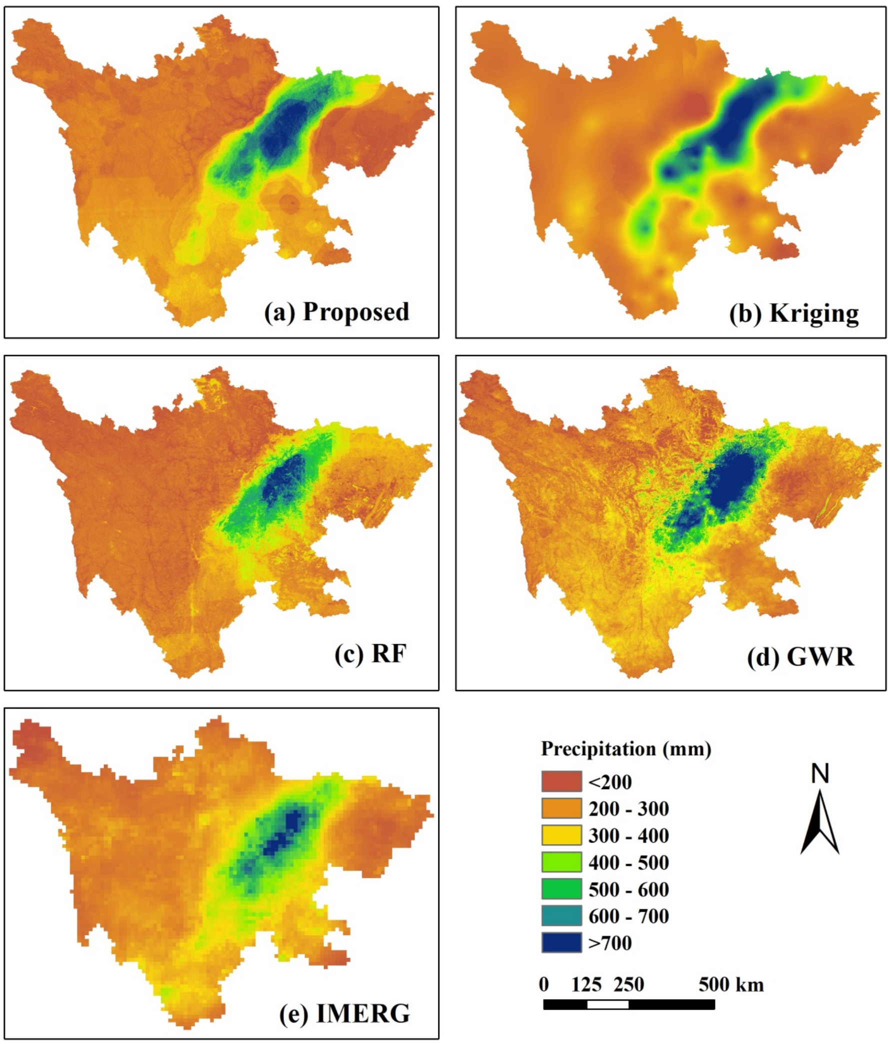

Fig. 12 Downscaled and calibrated precipitation comparison between the proposed

https://doi.org/10.5194/hess-2021-332
Preprint. Discussion started: 1 July 2021

method and some representative methods on the wettest month

5. Discussion

For downscaling and calibration of satellite-based precipitation, the three most important factors are model, predictors and temporal scale used for constructing predictors-precipitation relationship (Chen et al., 2020b). Thus, they should be carefully selected to produce accurate precipitation data.

5.1. Model

In previous studies, the most commonly adopted model is GWR (Chen et al., 2015; Xu et al., 2015), since it has the merit of taking the spatial variation between the predictors and precipitation into account. However, the performance of GWR seriously depends on the density of rain gauge stations, and large interpolation errors can be found in areas with sparse gauge stations and complex terrain characteristics (Lu et al., 2019). Ma et al. (2017) indicated that GWR-based downscaled TRMMs before and after residual correction for the period 2000 to 2013 at an annual scale are less accurate than the original TRMM over the Tibet Plateau. Karbalaye Ghorbanpour et al. (2021) showed that GWR has poorer downscaling results than the original TRMM for 2012 and 2013 on an annual scale over Lake Urmia Basin. Our results demonstrated that on a monthly scale (Fig. 5), GWR produces worse results than the original IMERG, with the RMSE, MAE and CC values of 38.77 mm, 22.71 mm and 0.907, respectively. On a seasonal scale (Table 1), GWR is less accurate than IMERG in summer, with the RMSE, MAE and CC values of 65.49 mm, 46.32 mm and 0.795, respectively. On an annual scale (Fig. 11), compared to IMERG, the performance of GWR is unsatisfactory in terms of CC. Moreover, the precipitation map of GWR shows some larger values compared to their neighbors (Fig. 12d).

In contrast, the ML methods including RF and SRF are always more accurate than GWR due to their merits for handling the complex nonlinear predictors-precipitation relationship. This conclusion agrees well with previous studies (Karbalaye Ghorbanpour et al., 2021; Sachindra et al., 2018). In addition, the ML methods do not require residual correction (Jing et al., 2016; Shi et al., 2015). However, as a statistical tool, the classical ML methods neglected the spatial autocorrelation between the gauge measurements. Thus, a spatial RF (SRF) with the consideration of the spatial autocorrelation information was constructed. SRF was used in both downscaling and calibration in our study, where the original IMERG and the gauge data were interpolated to produce input predictors for the first and second stages, respectively. The results on the three scales demonstrated the higher accuracy of SRF than RF (see Figs. 5-11, Table 1). Note that although kriging interpolation based on only gauge measurements is more accurate than IMERG, BPNN and GWR, its precipitation map is so smooth that many detailed precipitation patterns are lost (Fig. 12b).

5.2. Environmental predictors

NDVI, latitude, longitude and DEM-based parameters were commonly adopted environmental variables for estimating precipitation (Shi et al., 2015). However,

https://doi.org/10.5194/hess-2021-332
Preprint. Discussion started: 1 July 2021

satellite-based precipitation across regions with no relationship with NDVI and DEM could not be estimated. For example, in barren or snow areas, the precipitation does not influence NDVI due to the sparse distribution of vegetation (Xu et al., 2015). Jing et al. (2016) indicated that the downscaled models including LST features (LSTs) performed better those without LSTs. Thus, in addition to NDVI and DEM-related parameters, daytime LST (LST_D), nighttime LST (LST_N), and difference between day and night LSTs (LST_{D-N}) were also used in our study.

Based on RF (Breiman, 2001), the relative importance of each predictor (i.e. predictor importance estimate) is shown in Fig. 13. Results show that precipitation from kriging interpolation has the most importance, which indicates the significance of the spatial autocorrelation between gauge measurements. Kriging estimation is followed by downscaled precipitation. The three LSTs also have a great impact on the precipitation estimation, where LST_D seems more important than LST_N and LST_{D-N}. NDVI has a slight effect on the precipitation, which ranks last but one. This might be due to the fact that NDVI is influenced by both precipitation and temperature in the study site, and the low temperature above certain elevations hinders the vegetation growth. Motivated by this idea, Wang et al. (2019) first removed the influence of temperature on NDVI, and then used the processed NDVI for downscaling TRMA in Qilian Mountains. Different from the aforementioned scheme, we took both LSTs and NDVI as the predictors, and then the complex predictors-precipitation relationship was captured by RF based on its powerful learning ability. Among the 12 predictors, aspect has the least importance. This

https://doi.org/10.5194/hess-2021-332
Preprint. Discussion started: 1 July 2021

conclusion was also obtained by Ma et al. (2017) for downscaling TMPA 3B43 V7 data over the Tibet Plateau. Compared to aspect, DEM and terrain slope seem more important.

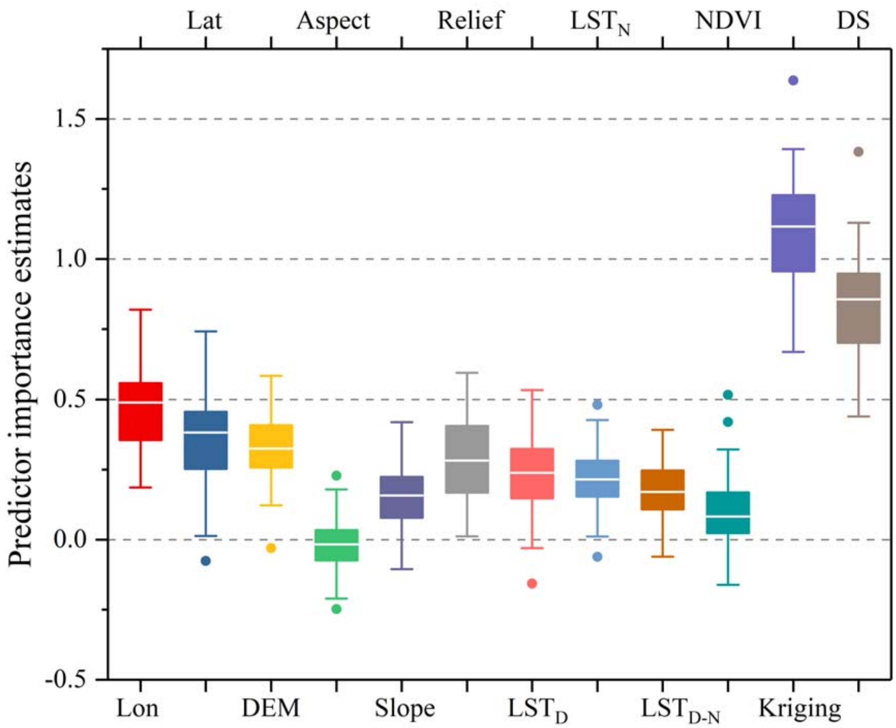

Fig. 13 Predictor importance estimates (Lat: latitude; Lon: longitude; DS: downscaled precipitation; kriging: interpolated precipitation based kriging on gauge data)

5.3. Temporal scale

Temporal scale has a great effect on the selection of predictors for precipitation estimation. There is a debate on whether NDVI should be taken as a predictor for downscaling and calibration of monthly precipitation. Some (Duan and Bastiaanssen, 2013; Immerzeel et al., 2009) argued that NDVI cannot be used for monthly

https://doi.org/10.5194/hess-2021-332
Preprint. Discussion started: 1 July 2021

precipitation estimation since the response of NDVI to precipitation usually delayed for two or three months. Hence, one effective solution is to perform downscaling at the annual scale, and then use the monthly fractions derived from the original precipitation data to disaggregate the annual precipitation to the monthly one (i.e. annual-based fraction disaggregation) (Duan and Bastiaanssen, 2013). However, some (Brunsell, 2006; Chen et al., 2020c; Lu et al., 2019; Xu et al., 2015) stated that the precipitation-NDVI relationship is hardly time-delayed, since vegetation could influence precipitation by adjusting temperature and air moisture during the growing seasons. Thus, it is possible to estimate precipitation with NDVI at the monthly scale. In our study, we found that the proposed method on the monthly scale is slightly more accurate than that on the annual scale (i.e. SRFdis) in all seasons (see Figs. 8-10), indicating that NDVI could be used for monthly precipitation estimates in the study site.

5.4. Easy-to-use feature

Since the classical RF does not consider the spatial information in the modeling process, Hengl et al. (2018) proposed an improved RF for spatial estimation, where the buffer distances from the point-based measurements were taken as the predictors. Motivated by this idea, Baez-Villanueva et al. (2020) presented a RF-based method (RF-MEP) for merging satellite precipitation products and rain gauge measurements, where the spatial distances from all rain gauges to the grid cells in the study site were used as the variables. RF-MEP performed better than all precipitation products and some merging methods. However, as stated by Baez-Villanueva et al. (2020), RF-MEP has a huge computational cost, since the number of extra input features equals to that of gauge measurements. Moreover, RF-MEP ignored the spatial autocorrelation between the gauge measurements. In comparison, our SRF only requires one extra feature that is estimated by kriging interpolation on the precipitation measurements. Compared to the buffer distance layers, it is much more computationally effective. Moreover, with the variogram-based kriging interpolation, the spatial autocorrelations between the gauge measurements and between the estimated precipitation and gauge measurements are taken into account. Thus, the aforementioned features make our method accurate, effective and easy-to-use.

Recently, Georganos et al. (2019) proposed a geographical RF to overcome spatial heterogeneity in remote sensing and population modelling. The geographical RF is essentially a local interpolation method, where only the *n* nearest observations around the interpolated point is used. However, this kind of methods has the tendency to produce discontinuity maps due to the local interpolation nature (Chen and Li, 2019). Moreover, the global information inherent in the dataset cannot be used, which might result in biased results. In comparison, our method with the aforementioned features is highly recommended.

5.5. Further researches

In the further studies, we will focus on the following directions. Firstly, other land surface variables such as soil moisture (Brocca et al., 2019; Fan et al., 2019), and meteorological conditions such as cloud properties (Sharifi et al., 2019) could be adopted to enhance the predictors-precipitation relationship, thereby further improving IMERG quality. Secondly, the correction of satellite-based precipitation on higher-temporal scales (e.g. daily or hourly) is challenging and valuable (Chen et al., 2020b; R. Lima et al., 2021; Sun and Lan, 2021; Wu et al., 2020). Whether our method could be applied on these scales might need validation. Thirdly, in our experiments, all rain gauge measurements were used to improve the quality of satellite-based precipitation. However, it is generally accepted that sample density has a significant effect on the accuracy of the classical calibration methods (Baez-Villanueva et al., 2020; Bai et al., 2019; Lin and Wang, 2011; Wang and Lin, 2015; Zhang et al., 2021). Thus, its influence on the results of our method should be quantitatively assessed, thereby determining the most suitable gauge density in different hydrological applications. Finally, numerous satellite-based precipitation products have been available, and each one has its shortcomings and advantages for the capture of spatial precipitation patterns (Baez-Villanueva et al., 2020; Chen et al., 2020c). Thus, the fusion of multiple precipitation products based on our methodology is a promising alternative to improve the quality of precipitation data. Thus, its performance requires further assessment.

6. Conclusions

To enhance the resolution (from 0.1° to 1 km) and accuracy of the monthly IMERG V06B Final Run product, a spatial RF (SRF)-based downscaling and calibration

https://doi.org/10.5194/hess-2021-332
Preprint. Discussion started: 1 July 2021

Hydrology and Earth System Sciences
Open Access
Discussions

method is proposed in this paper. The merits of the proposed method are twofold: (i) SRF takes the spatial autocorrelation between the precipitation measurements into account when constructing the predictors-precipitation relationship and (ii) the SRF model is used not only in downscaling but also in calibration of IMERG, with the incorporation of some precipitation-related high-resolution variables. The performance of the proposed method was compared with those of seven methods including GWR, RF, BPNN, Bi-SRF, SRF-GDA, SRFdis and kriging for enhancing the quality and resolution of monthly IMERG across Sichuan province, China from 2015 to 2019. The main findings and conclusions can be summarized as follows:

(1) The SRF-based methods including the proposed method, Bi-SRF, SRF-GDA and SRFdis are more accurate than the classical methods on all temporal scales. Moreover, the proposed method ranks the first, indicating that SRF-based downscaling and calibration is more promising than bilinear-based downscaling and GDA-based calibration.

(2) The comparison between the monthly-based and annual-based estimation demonstrates that there is no statistically significant difference between them, indicating that NDVI can be used for monthly precipitation estimation in the study site.

(3) Kriging outperforms the original IMERG, BPNN and GWR in terms of RMSE, MAE and CC. However, its interpolation map suffers from serious loss of spatial variation of precipitation, since it only uses the gauge measurements.

(4) Based on the variable importance assessment of RF, the precipitation interpolated

https://doi.org/10.5194/hess-2021-332
Preprint. Discussion started: 1 July 2021

by kriging on the gauge measurements is the most important variable, whereas terrain aspect is the least one.

Overall, the proposed methodology is general, robust, accurate and easy-to-use, since its promising performance in the study area with an obvious heterogeneity in terrain morphology and precipitation. Thus, it can be easily applied to other regions, where high resolution and accurate precipitation data is urgently required.

Data availability

The gauge data are from the China Meteorological Data Service Center (http://data.cma.cn, last access: January 2021). The GPM data are from https://gpm.nasa.gov/data (last access: January 2021). The GPM data are from http://srtm.csi.cgiar.org/ (last access: January 2021). The MOD13A3 data are from http://www.gscloud.cn/ (last access: January 2021). The MOD11A2 data are from https://ladsweb.modaps.eosdis.nasa.gov (last access: January 2021).

Declaration of Competing Interest

The authors declare that they have no known competing financial interests or personal relationships that could have appeared to influence the work reported in this paper.

Author contributions

CF and YY conceived the idea, and acquired the project and financial support. BJ conducted the detailed analysis. CF contributed to the writing and revisions.

Competing interests

The authors declare that they have no conflict of interest.

Acknowledgement

This work was supported by the National Natural Science Foundation of China (Grant No. 41804001), Shandong Provincial Natural Science Foundation, China (Grant No. ZR2020YQ26, ZR2019MD007, ZR2019BD006), A Project of Shandong Province Higher Educational Youth Innovation Science and Technology Program (Grant No. 2019KJH007), Shandong Provincial Key Research and Development Program (Major Scientific and Technological Innovation Project) (Grant No. 2019JZZY010429) and by the Scientific Research Foundation of Shandong University of Science and Technology for Recruited Talents (Grant No. 2019RCJJ003).

References

An, S., Liu, W., Venkatesh, S., 2007. Fast cross-validation algorithms for least squares support vector machine and kernel ridge regression. Pattern Recognit., 40 (8), 2154-2162.

Ashouri, H., Hsu, K.-L., Sorooshian, S., Braithwaite, D.K., Knapp, K.R., Cecil, L.D., Nelson, B.R., Prat, O.P., 2015. PERSIANN-CDR: Daily Precipitation Climate Data Record from Multisatellite Observations for Hydrological and Climate Studies. Bulletin of the American Meteorological Society, 96 (1), 69-83.

Baez-Villanueva, O.M., Zambrano-Bigiarini, M., Beck, H.E., McNamara, I., Ribbe, L., Nauditt, A., Birkel, C., Verbist, K., Giraldo-Osorio, J.D., Xuan Thinh, N., 2020. RF-MEP: A novel Random Forest method for merging gridded precipitation products and ground-based measurements. Remote Sensing of Environment, 239, 111606.

Bai, X., Wu, X., Wang, P., 2019. Blending long-term satellite-based precipitation data with gauge observations for drought monitoring: Considering effects of different gauge densities. Journal of Hydrology, 577, 124007.

Beck, H.E., van Dijk, A.I.J.M., Levizzani, V., Schellekens, J., Miralles, D.G., Martens, B., de Roo, A., 2017. MSWEP: 3-hourly 0.25° global gridded precipitation (1979–2015) by merging gauge, satellite, and reanalysis data. Hydrology and Earth System Sciences, 21 (1), 589-615.

Beck, H.E., Wood, E.F., Pan, M., Fisher, C.K., Miralles, D.G., van Dijk, A.I.J.M., McVicar, T.R., Adler, R.F., 2019. MSWEP V2 Global 3-Hourly 0.1° Precipitation: Methodology and Quantitative Assessment. Bulletin of the American Meteorological Society, 100 (3), 473-500.

Belgiu, M., Drăguţ, L.J.I.J.o.P., Sensing, R., 2016. Random forest in remote sensing: A review of applications and future directions. 114, 24-31.

Berndt, C., Haberlandt, U., 2018. Spatial interpolation of climate variables in Northern Germany-Influence of temporal resolution and network density. Journal of Hydrology-Regional Studies, 15, 184-202.

Berndt, C., Rabiei, E., Haberlandt, U., 2014. Geostatistical merging of rain gauge and radar data for high temporal resolutions and various station density scenarios. Journal of Hydrology, 508, 88-101.

Bhuiyan, M.A.E., Nikolopoulos, E.I., Anagnostou, E.N., Quintana-Seguí, P., Barella-Ortiz, A., 2018. A nonparametric statistical technique for combining global precipitation datasets: development and hydrological evaluation over the Iberian Peninsula. Hydrology and Earth System Sciences, 22 (2), 1371-1389.

Bhuiyan, M.A.E., Yang, F., Biswas, N.K., Rahat, S.H., Neelam, T.J., 2020. Machine Learning-Based Error Modeling to Improve GPM IMERG Precipitation Product over the Brahmaputra River Basin. Forecasting, 2 (3), 248-266.

Breiman, L., 2001. Random Forests. Machine Learning, 45 (1), 5-32.

Brocca, L., Filippucci, P., Hahn, S., Ciabatta, L., Massari, C., Camici, S., Schüller, L., Bojkov, B., Wagner, W., 2019. SM2RAIN–ASCAT (2007–2018): global daily satellite rainfall data from ASCAT soil moisture observations. Earth System Science Data, 11 (4), 1583-1601.

Brunsell, N.A., 2006. Characterization of land-surface precipitation feedback regimes with remote sensing. Remote Sensing of Environment, 100 (2), 200-211.

Chao, L., Zhang, K., Li, Z., Zhu, Y., Wang, J., Yu, Z., 2018. Geographically weighted regression based methods for merging satellite and gauge precipitation. Journal of Hydrology, 558, 275-289.

Cheema, M.J.M., Bastiaanssen, W.G.M., 2012. Local calibration of remotely sensed rainfall from the TRMM satellite for different periods and spatial scales in the Indus Basin. International Journal of Remote Sensing, 33 (8), 2603-2627.

Chen, C., Li, Y., 2019. A fast global interpolation method for digital terrain model generation from large LiDAR-derived data. Remote Sensing, 11 (11), 1324.

Chen, C., Yang, S., Li, Y., 2020a. Accuracy Assessment and Correction of SRTM DEM using ICESat/GLAS Data under Data Coregistration. Remote Sensing, 12 (20), 3435.

Chen, C., Zhao, S., Duan, Z., Qin, Z., 2015. An Improved Spatial Downscaling Procedure for TRMM 3B43 Precipitation Product Using Geographically Weighted Regression. IEEE Journal of Selected Topics in Applied Earth Observations and Remote Sensing, 8 (9), 4592-4604.

Chen, F., Gao, Y., Wang, Y., Li, X., 2020b. A downscaling-merging method for high-resolution daily precipitation estimation. Journal of Hydrology, 581, 124414.

Chen, F., Liu, Y., Liu, Q., Li, X., 2014. Spatial downscaling of TRMM 3B43 precipitation considering spatial heterogeneity. International Journal of Remote Sensing, 35 (9), 3074-3093.

Chen, J., Brissette, F.P., Chaumont, D., Braun, M., 2013. Finding appropriate bias correction methods in downscaling precipitation for hydrologic impact studies over North America. Water Resources Research, 49 (7), 4187-4205.

Chen, S.-T., Yu, P.-S., Tang, Y.-H., 2010. Statistical downscaling of daily precipitation using support vector machines and multivariate analysis. Journal of Hydrology, 385 (1), 13-22.

Chen, S., Xiong, L., Ma, Q., Kim, J.-S., Chen, J., Xu, C.-Y., 2020c. Improving daily spatial precipitation estimates by merging gauge observation with multiple satellite-based precipitation products based on the geographically weighted ridge regression method. Journal of Hydrology, 589, 125156.

Chen, Y., Huang, J., Sheng, S., Mansaray, L.R., Liu, Z., Wu, H., Wang, X., 2018. A new downscaling-integration framework for high-resolution monthly precipitation estimates: Combining rain gauge observations, satellite-derived precipitation data and geographical ancillary data. Remote Sensing of Environment, 214, 154-172.

Duan, Z., Bastiaanssen, W.G.M., 2013. First results from Version 7 TRMM 3B43 precipitation product in combination with a new downscaling–calibration procedure. Remote Sensing of Environment, 131, 1-13.

Elnashar, A., Zeng, H., Wu, B., Zhang, N., Tian, F., Zhang, M., Zhu, W., Yan, N., Chen, Z., Sun, Z., Wu, X., Li, Y., 2020. Downscaling TRMM Monthly Precipitation Using Google Earth Engine and Google Cloud Computing. Remote Sensing, 12 (23).

Fan, D., Wu, H., Dong, G., Jiang, X., Xue, H., 2019. A Temporal Disaggregation Approach for TRMM Monthly Precipitation Products Using AMSR2 Soil Moisture Data. Remote Sensing, 11 (24).

Funk, C., Peterson, P., Landsfeld, M., Pedreros, D., Verdin, J., Shukla, S., Husak, G., Rowland, J., Harrison, L., Hoell, A., Michaelsen, J., 2015. The climate hazards infrared precipitation with stations—a new environmental record for monitoring extremes. Scientific Data, 2 (1), 150066.

Gebregiorgis, A.S., Hossain, F., 2013. Understanding the Dependence of Satellite Rainfall Uncertainty on Topography and Climate for Hydrologic Model Simulation. IEEE Transactions on Geoscience and Remote Sensing, 51 (1), 704-718.

Georganos, S., Grippa, T., Niang Gadiaga, A., Linard, C., Lennert, M., Vanhuysse, S., Mboga, N., Wolff, E., Kalogirou, S., 2019. Geographical random forests: a spatial extension of the random forest algorithm to address spatial heterogeneity in remote sensing and population modelling. Geocarto International, 1-16.

Goovaerts, P., 2000. Geostatistical approaches for incorporating elevation into the spatial interpolation of rainfall. J. Hydrol. , 228 (1-2), 113-129.

Haile, A.T., Habib, E., Rientjes, T., 2013. Evaluation of the climate prediction center (CPC) morphing technique (CMORPH) rainfall product on hourly time scales over the source of the Blue Nile River. Hydrological Processes, 27 (12), 1829-1839.

Hengl, T., Nussbaum, M., Wright, M.N., Heuvelink, G.B., Gräler, B.J.P., 2018. Random forest as a generic framework for predictive modeling of spatial and spatio-temporal variables. PeerJ, 6, e5518.

Hou, A.Y., Kakar, R.K., Neeck, S., Azarbarzin, A.A., Kummerow, C.D., Kojima, M., Oki, R., Nakamura, K., Iguchi, T., 2014. The Global Precipitation Measurement Mission. Bulletin of the American Meteorological Society, 95 (5), 701-722.

Huffman, G., Bolvin, D., Braithwaite, D., Hsu, K., Joyce, R., 2019. Algorithm theoretical basis document (ATBD) NASA global precipitation measurement (GPM) integrated multi-satellitE Retrievals for GPM (IMERG). Nasa (December), 29.

Huffman, G.J., Bolvin, D.T., Nelkin, E.J., Wolff, D.B., Adler, R.F., Gu, G., Hong, Y., Bowman, K.P., Stocker, E.F., 2007. The TRMM Multisatellite Precipitation Analysis (TMPA): Quasi-Global, Multiyear, Combined-Sensor Precipitation Estimates at Fine Scales. Journal of Hydrometeorology, 8 (1), 38-55.

Immerzeel, W.W., Rutten, M.M., Droogers, P., 2009. Spatial downscaling of TRMM precipitation using vegetative response on the Iberian Peninsula. Remote Sensing of Environment, 113 (2), 362-370.

Jia, S., Zhu, W., Lű, A., Yan, T., 2011. A statistical spatial downscaling algorithm of TRMM precipitation based on NDVI and DEM in the Qaidam Basin of China. remote sensing of environment, 115 (12), 3069-3079.

https://doi.org/10.5194/hess-2021-332
Preprint. Discussion started: 1 July 2021

Jing, W., Yang, Y., Yue, X., Zhao, X., 2016. A Spatial Downscaling Algorithm for Satellite-Based Precipitation over the Tibetan Plateau Based on NDVI, DEM, and Land Surface Temperature. Remote Sensing, 8 (8).

Karbalaye Ghorbanpour, A., Hessels, T., Moghim, S., Afshar, A., 2021. Comparison and assessment of spatial downscaling methods for enhancing the accuracy of satellite-based precipitation over Lake Urmia Basin. Journal of Hydrology, 596, 126055.

Li, M., Shao, Q., 2010. An improved statistical approach to merge satellite rainfall estimates and raingauge data. Journal of Hydrology, 385 (1), 51-64.

Li, T., Shen, H., Yuan, Q., Zhang, X., Zhang, L., 2017. Estimating ground‐level PM2.5 by fusing satellite and station observations: a geo-intelligent deep learning approach. Geophysical Research Letters, 44 (23), 11,985-911,993.

Li, Y., Zhang, Y., He, D., Luo, X., Ji, X., 2019. Spatial Downscaling of the Tropical Rainfall Measuring Mission Precipitation Using Geographically Weighted Regression Kriging over the Lancang River Basin, China. Chinese Geographical Science, 29 (3), 446-462.

Lin, A., Wang, X.L., 2011. An algorithm for blending multiple satellite precipitation estimates with in situ precipitation measurements in Canada. Journal of Geophysical Research: Atmospheres, 116 (D21).

Lu, X., Tang, G., Wang, X., Liu, Y., Jia, L., Xie, G., Li, S., Zhang, Y., 2019. Correcting GPM IMERG precipitation data over the Tianshan Mountains in China. Journal of Hydrology, 575, 1239-1252.

Lu, X., Tang, G., Wang, X., Liu, Y., Wei, M., Zhang, Y., 2020. The Development of a Two-Step Merging and Downscaling Method for Satellite Precipitation Products. Remote Sensing, 12 (3).

Ma, Z., Shi, Z., Zhou, Y., Xu, J., Yu, W., Yang, Y., 2017. A spatial data mining algorithm for downscaling TMPA 3B43 V7 data over the Qinghai–Tibet Plateau with the effects of systematic anomalies removed. Remote Sensing of Environment, 200, 378-395.

https://doi.org/10.5194/hess-2021-332
Preprint. Discussion started: 1 July 2021

Hydrology and Earth System Sciences
Open Access
Discussions

Mohsenzadeh Karimi, S., Kisi, O., Porrajabali, M., Rouhani-Nia, F., Shiri, J., 2020. Evaluation of the support vector machine, random forest and geo-statistical methodologies for predicting long-term air temperature. ISH Journal of Hydraulic Engineering, 26 (4), 376-386.

Park, N.-W., Kyriakidis, P.C., Hong, S., 2017. Geostatistical Integration of Coarse Resolution Satellite Precipitation Products and Rain Gauge Data to Map Precipitation at Fine Spatial Resolutions. Remote Sensing, 9 (3), 255.

Pham, B.T., Le, L.M., Le, T.-T., Bui, K.-T.T., Le, V.M., Ly, H.-B., Prakash, I., 2020. Development of advanced artificial intelligence models for daily rainfall prediction. Atmospheric Research, 237, 104845.

R. Lima, C.H., Kwon, H.-H., Kim, Y.-T., 2021. A Bayesian Kriging Model Applied for Spatial Downscaling of Daily Rainfall from GCMs. Journal of Hydrology, 126095.

Sachindra, D.A., Ahmed, K., Rashid, M.M., Shahid, S., Perera, B.J.C., 2018. Statistical downscaling of precipitation using machine learning techniques. Atmospheric Research, 212, 240-258.

Sharifi, E., Saghafian, B., Steinacker, R., 2019. Downscaling Satellite Precipitation Estimates With Multiple Linear Regression, Artificial Neural Networks, and Spline Interpolation Techniques. Journal of Geophysical Research Atmospheres, 124 (2), 789-805.

Shi, Y., Song, L., Xia, Z., Lin, Y., Myneni, R.B., Choi, S., Wang, L., Ni, X., Lao, C., Yang, F., 2015. Mapping Annual Precipitation across Mainland China in the Period 2001–2010 from TRMM3B43 Product Using Spatial Downscaling Approach. Remote Sensing, 7 (5), 5849-5878.

Sun, L., Lan, Y., 2021. Statistical downscaling of daily temperature and precipitation over China using deep learning neural models: Localization and comparison with other methods. International Journal of Climatology, 41 (2), 1128-1147.

Tao, Y., Gao, X., Hsu, K., Sorooshian, S., Ihler, A., 2016. A Deep Neural Network Modeling Framework to Reduce Bias in Satellite Precipitation Products. Journal of Hydrometeorology, 17 (3), 931-945.

Ullah, S., Zuo, Z., Zhang, F., Zheng, J., Huang, S., Lin, Y., Iqbal, I., Sun, Y., Yang, M., Yan, L., 2020. GPM-Based Multitemporal Weighted Precipitation Analysis Using GPM_IMERGDF Product and ASTER DEM in EDBF Algorithm. Remote Sensing, 12 (19).

Wang, L., Chen, R., Han, C., Yang, Y., Liu, J., Liu, Z., Wang, X., Liu, G., Guo, S., 2019. An Improved Spatial–Temporal Downscaling Method for TRMM Precipitation Datasets in Alpine Regions: A Case Study in Northwestern China's Qilian Mountains. Remote Sensing, 11 (7).

Wang, X., Lin, A., 2015. An algorithm for integrating satellite precipitation estimates with in situ precipitation data on a pentad time scale. Journal of Geophysical Research: Atmospheres, 120 (9), 3728-3744.

Wu, H., Yang, Q., Liu, J., Wang, G., 2020. A spatiotemporal deep fusion model for merging satellite and gauge precipitation in China. Journal of Hydrology, 584, 124664.

Wu, Z., Zhang, Y., Sun, Z., Lin, Q., He, H., 2018. Improvement of a combination of TMPA (or IMERG) and ground-based precipitation and application to a typical region of the East China Plain. Science of The Total Environment, 640-641, 1165-1175.

Xie, P., Xiong, A.-Y., 2011. A conceptual model for constructing high-resolution gauge-satellite merged precipitation analyses. Journal of Geophysical Research: Atmospheres, 116 (D21).

Xu, S., Wu, C., Wang, L., Gonsamo, A., Shen, Y., Niu, Z., 2015. A new satellite-based monthly precipitation downscaling algorithm with non-stationary relationship between precipitation and land surface characteristics. Remote Sensing of Environment, 162, 119-140.

Yan, X., Chen, H., Tian, B., Sheng, S., Wang, J., Kim, J.-S., 2021. A Downscaling–Merging Scheme for Improving Daily Spatial Precipitation Estimates Based on Random Forest and Cokriging. Remote Sensing, 13 (11), 2040.

Hydrology and Earth System Sciences
Open Access
Discussions

Yang, Y., Luo, Y., 2014. Using the Back Propagation Neural Network Approach to Bias Correct TMPA Data in the Arid Region of Northwest China. Journal of Hydrometeorology, 15 (1), 459-473.

Yang, Z., Hsu, K., Sorooshian, S., Xu, X., Braithwaite, D., Zhang, Y., Verbist, K.M.J., 2017. Merging high‐resolution satellite‐based precipitation fields and point‐scale rain gauge measurements—A case study in Chile. Journal of Geophysical Research: Atmospheres, 122 (10), 5267-5284.

Zambrano-Bigiarini, M., Nauditt, A., Birkel, C., Verbist, K., Ribbe, L., 2017. Temporal and spatial evaluation of satellite-based rainfall estimates across the complex topographical and climatic gradients of Chile. Hydrol. Earth Syst. Sci., 21 (2), 1295-1320.

Zhang, L., Li, X., Zheng, D., Zhang, K., Ma, Q., Zhao, Y., Ge, Y., 2021. Merging multiple satellite-based precipitation products and gauge observations using a novel double machine learning approach. Journal of Hydrology, 594.

Zhang, X., Tang, Q., 2015. Combining satellite precipitation and long-term ground observations for hydrological monitoring in China. Journal of Geophysical Research: Atmospheres, 120 (13), 6426-6443.

Zhao, T., Yatagai, A., 2014. Evaluation of TRMM 3B42 product using a new gauge-based analysis of daily precipitation over China. International Journal of Climatology, 34 (8), 2749-2762.